Extracellular vesicles released by keratinocytes regulate melanosome maturation, melanocyte dendricity, and pigment transfer

Marie-Thérèse Prospéri, Cécile Giordano, Mireia Gomez-Duro, Ilse Hurbain, Anne-Sophie Macé, Graça Raposo, Gisela D'angelo

PNAS RESEARCH ARTICLE | CELL BIOLOGY OPEN ACCESS

Extracellular vesicles released by keratinocytes regulate melanosome maturation, melanocyte dendricity, and pigment transfer

Marie-Thérèse Prospéri[a], Cécile Giordano[a], Mireia Gomez-Duro[a], Ilse Hurbain[a,b], Anne-Sophie Macé[a,b], Graça Raposo[a,b], and Gisela D'Angelo[a,1]

Edited by Marianne Bronner, California Institute of Technology, Pasadena, CA; received December 6, 2023; accepted March 7, 2024

Extracellular vesicles (EVs) facilitate the transfer of proteins, lipids, and genetic material between cells and are recognized as an additional mechanism for sustaining intercellular communication. In the epidermis, the communication between melanocytes and keratinocytes is tightly regulated to warrant skin pigmentation. Melanocytes synthesize the melanin pigment in melanosomes that are transported along the dendrites prior to the transfer of melanin pigment to keratinocytes. EVs secreted by keratinocytes modulate pigmentation in melanocytes [(A. Lo Cicero *et al.*, *Nat. Commun.* 6, 7506 (2015)]. However, whether EVs secreted by keratinocytes contribute to additional processes essential for melanocyte functions remains elusive. Here, we show that keratinocyte EVs enhance the ability of melanocytes to generate dendrites and mature melanosomes and promote their efficient transfer. Further, keratinocyte EVs carrying Rac1 induce important morphological changes, promote dendrite outgrowth, and potentiate melanin transfer to keratinocytes. Hence, in addition to modulating pigmentation, keratinocytes exploit EVs to control melanocyte plasticity and transfer capacity. These data demonstrate that keratinocyte-derived EVs, by regulating melanocyte functions, are major contributors to cutaneous pigmentation and expand our understanding of the mechanism underlying skin pigmentation via a paracrine EV-mediated communication.

small extracellular vesicles | melanocytes | dendrites | pigment transfer | skin pigmentation

Significance

Our work uncovers how keratinocyte-derived EVs (Extracellular vesicles) control melanocyte physiology and functions. By promoting the growth of melanocyte dendrites, maturation, accumulation and peripheral positioning of pigmented melanosomes within the dendrites, and transfer of melanin to keratinocytes, EVs released by keratinocytes control crucial processes in skin photoprotection. Importantly, given that dysregulation of these pathways could underlie pigment disorders, melanoma or skin carcinoma, our results open avenues to exploit keratinocyte EVs as tools for the design of advanced therapies to enhance the ability of melanocytes to provide skin photoprotection and thus decrease the incidence of pigmentary disorders and skin cancers.

Skin pigmentation results from the communication between two distinct cell types of the epidermis, namely the pigment producing melanocytes located in the epidermal basal layer and the pigment receiving keratinocytes that are more superficially distributed. Together, they form the epidermal melanin unit in which one melanocyte through its dendrites contacts around 30 to 40 keratinocytes (1). This cell–cell physical proximity facilitates the transfer of melanin from melanocytes to the keratinocyte and contributes to skin color and photoprotection against ultraviolet (UV) solar radiations (2).

Melanin is synthesized in melanosomes, a lysosome-related organelle, which undergoes maturation through four distinct stages (from early nonpigmented stages I/II to melanized stages III/IV) (3, 4). Maturing pigmented melanosomes undergo microtubule- and F-actin-dependent transport to the tip of melanocyte dendrites where they are captured by actin-related machineries, including the actin-based motor protein Myosin Va (Myo Va), prior to the transfer of melanin pigment to keratinocytes (5–7). Melanosome maturation, dendrite formation, and melanosome transfer are stimulated by hormones secreted by keratinocytes including α-melanocyte-stimulating hormone, endothelin-1 (ET-1), and nerve growth factors, as well as ultraviolet radiation. These hormones and exposure to ultraviolet solar radiation activate various signaling pathways, including cyclic adenosine monophosphate (cAMP)/protein kinase A (PKA), protein kinase C (PKC) and mitogen-activated protein kinase (MAPK) (8–12), which not only enhance pigment synthesis, but also lead to a reorganization of the cytoskeleton. This reorganization involves a reduction in guanosine-5'-triphosphate (GTP)-bound Rho levels and an increase in Rac1-GTP levels, which promotes dendrite formation (13–15).

Apart from these soluble factors, keratinocytes release extracellular vesicles (EVs) that facilitate communication between keratinocytes and other skin cells, i.e., fibroblasts and melanocytes (16–18). EVs are membrane-bound vesicles that originate from the outward budding of the plasma membrane (ectosomes or large EVs) or from the endosomal network [exosomes or small EVs (sEVs)]. EVs carry a variety of proteins, lipids, and genetic material [mRNA, microRNAs (miRNAs)] that once transferred to recipient cells, activate different signaling pathways, and modulate their fate and behavior (19, 20). In the skin, keratinocyte-derived sEVs with features of endosome-derived exosomes were shown to modulate melanocyte pigmentation (17, 21, 22). However, the cellular and molecular mechanisms underlying additional functions of sEVs and essential processes that

Author affiliations: [a]Institut Curie, Paris Sciences & Letters Research University, CNRS, UMR144, Structure and Membrane Compartments, Paris Cedex 05 75248, France; and [b]Institut Curie, Paris Sciences & Letters Research University, CNRS, UMR144, Cell and Tissue Imaging Facility (The Cell and Tissue Imaging Platform (PICT-IBiSA)), Paris Cedex 05 75248, France

Author contributions: G.D. designed research; M.-T.P., C.G., M.G.-D., and I.H. performed research; A.-S.M. contributed new reagents/analytic tools; M.-T.P., C.G., M.G.-D., I.H., G.R., and G.D. analyzed data; and M.-T.P. and G.D. wrote the paper.

The authors declare no competing interest.

This article is a PNAS Direct Submission.

[1]To whom correspondence may be addressed. Email: gisela.dangelo@curie.fr.

This article contains supporting information online at https://www.pnas.org/lookup/suppl/doi:10.1073/pnas.2321323121/-/DCSupplemental.

Published April 12, 2024.

contribute to skin pigmentation, beyond melanin synthesis, remain to be determined.

Here, we have isolated sEVs with features of endosome-derived exosomes (17) and adopted the current nomenclature of sEVs according to the MISEV guidelines (23). We have investigated sEVs secreted by primary human epidermal keratinocytes (HEKs) to delineate their functional impact on primary human epidermal melanocyte (HEM) activation. We show that HEK sEVs induce a drastic increase in the proportion of pigmented melanosomes and promote their peripheral accumulation. They also promote an increase of MyoVa at the tip of HEM dendrites and enhance melanin transfer ability. Furthermore, we found that HEK sEVs induce morphological remodeling of the HEM plasma membrane and the formation of numerous dendrites, a process that is mediated by Rac1-containing sEVs. Overall, this study put forward unique functions of HEK sEVs, at least through their Rac1 content, in skin pigmentation by controlling the formation of pigmented and transfer-competent dendrites, crucial for the pigment transfer to HEKs.

Results

Keratinocyte sEVs Promote Pigment Transfer from Melanocytes to Keratinocytes. Skin pigmentation and photoprotection rely on sequential processes that involve synthesis of melanin in HEMs, followed by its transfer to adjacent epidermal HEKs (24). Recent reports have shown that sEVs released by HEKs enhance melanin synthesis in HEMs (17, 21, 22). To investigate whether these sEVs facilitate melanin pigment transfer from HEMs to HEKs, we first isolated sEVs from HEKs of light (HEK-L) and dark (HEK-D) pigmented skin types and characterized these sEVs according to the MISEV guidelines (23) (*SI Appendix*, Fig. S1 and *Materials and Methods*). Immunoblotting of both sEV fractions was positive for classical sEV markers (Alix, CD63, TSG101, and Syntenin), some of which were enriched compared to the corresponding whole-cell lysates (L) and tubulin protein levels (*SI Appendix*, Fig. S1*A*). HEK-sEV fractions were devoid of intracellular contaminants as evidenced by the absence of the calnexin, an endoplasmic reticulum resident protein (*SI Appendix*, Fig. S1*A*). Nanoparticle tracking analysis (NTA) revealed that both sEV fractions displayed a similar concentration of particles (*SI Appendix*, Fig. S1*B*). Further visualization of the sEV fractions using transmission electron microscopy (TEM) with negative staining showed that both fractions contained a mixture of cup-shaped sEVs, with various electron densities (*SI Appendix*, Fig. S1*C*), however, with similar diameter (sEV-L: 86.6 ± 15.8 nm, sEV-D: 84.2 ± 18.9 nm; *SI Appendix*, Fig. S1*D*). By immuno-EM (IEM), we observed that both sEV fractions were similarly labeled for CD9, CD63, or CD81 sEV components (*SI Appendix*, Fig. S1*E*). We further separated the sEVs by velocity iodixanol (OptiPrep) density gradient to control for the presence of potential contaminants coisolated with sEVs during the ultracentrifugation (*SI Appendix*, Fig. S1*F*). We found that CD63 was present in two to three consecutive fractions (1.082 to 1.095 g/mL) whose concentrations range between 7×10^9 and 8.7×10^9 particles/ml for sEV-L or sEV-D, respectively (*SI Appendix*, Fig. S1*F*). These data show that independently of their skin phototypes, HEKs secrete a homogenous population of sEVs in similar quantity and quality.

Next, we investigated the functional effects of HEK sEVs on the transfer of melanin pigment from HEMs to HEKs. HEM-HEK were cocultured, and we analyzed the transferred pigments by immunofluorescence microscopy (IFM). HEMs previously incubated for 48 h or not with HEK-sEVs were cocultured with HEKs for 48 h, chemically fixed, and colabeled with anti-epidermal growth factor receptor (EGFR) antibody (staining HEKs; green) and HMB45 antibody (staining premelanosome protein (PMEL) fibrils onto which melanin deposits; red) (25). Note that melanized HEMs are strongly labeled for HEM45 as compared to transferred melanin pigment in HEKs (Fig. 1*A*). When HEKs were cocultured with sEVs-incubated HEMs (Fig. 1 *A*, *Right*), the proportion of HEKs positive for at least one HMB45-positive structure was substantially increased nearly twofold compared to control conditions [PBS (phosphate-buffered saline): 30% ± 1.5%; sEVs: 60% ± 3.2%, Fig. 1*B*]. This points toward the ability of sEVs to enhance the transfer of melanin pigment from HEMs to HEKs. To reinforce this observation, and as more than one HBM45-positive structure can be transferred to HEKs, we measured the surface area covered by HMB45-positive structures and normalized it to the cell surface area (*Materials and Methods*). The significant increase of the area covered by HMB45-positive structures per HEKs cocultured with sEV-incubated HEMs indicates that a higher number of HMB45-positive structures were transferred to each HEK compared to control (Fig. 1*C*). Taken together, these data show that sEV-treated HEMs exhibit enhanced melanin transfer capacity, allowing a greater number of neighboring HEKs to obtain more melanin pigment, and further indicate that sEVs released by HEKs are facilitators of melanin transfer.

Keratinocyte sEVs Promote Melanosome Maturation, Peripheral Accumulation, and an Increase of Myo Va at the Tip of Melanocyte Dendrites. Given that melanosome maturation, accumulation and capture at the dendritic tips are critical steps preceding melanin pigment transfer to neighboring HEKs, we set out to examine whether these processes are also affected by HEK sEVs. HEMs were incubated for 48 h with PBS or HEK sEVs (sEVs) from donors of the same phenotype and maturation of melanosomes was analyzed by TEM. Melanosome stages, from unpigmented (stage I and II) to pigmented stages (stage III and IV), were defined based on their morphology and melanin content (*SI Appendix*, Fig. S2*A*). We observed that mature melanosomes (late stages) were distributed throughout the dendrites of sEV-treated HEMs (*SI Appendix*, Fig. S2 *A* and *B*, *Right*), as compared to control, in which mostly unpigmented melanosomes (early stages) were seen (*SI Appendix*, Fig. S2 *A* and *B*, *Left*). Remarkably, sEV incubation promoted a significant decrease in the percentage of unpigmented melanosomes (58% ± 4.6%) concomitant with a 3.2-fold increase in the proportion of pigmented melanosomes (42% ± 4.6%) compared to control (Fig. 2 *A* and *B*). In contrast, in the absence of sEVs in the medium, the vast majority (90% ± 4%) consisted of unpigmented melanosomes (early stages) while only a small percentage (10% ± 4%) were pigmented (Fig. 2 *A* and *B*). When we examined in particular the distribution of melanosomes at the dendritic tips of control HEMs, we found only a small proportion of mature melanosomes (10% ± 5.1%). In contrast, exposure of HEMs to HEK sEVs for 48 h, triggered a striking increased (3.8-fold) in the percentage of pigmented melanosomes (48% ± 6%) at the dendritic tip, in the peripheral position, and in close proximity to the plasma membrane compared to unexposed cells (Fig. 2 *A*, *Upper* and Fig. 2*C*). Interestingly, the overall increase of pigmented melanosomes in sEV-incubated HEMs was similar to the increase of peripheral pigmented melanosomes at the tip of dendrites (Fig. 2 *B* and *C*).

Myo Va binds to F-actin filaments and facilitates thereby the positioning and anchoring of pigmented melanosomes at the dendritic tip previous to the transfer of melanin pigment to HEKs (5–7). We speculated that the accumulation of pigmented melanosomes at the dendritic tips of sEVs-treated HEMs might be

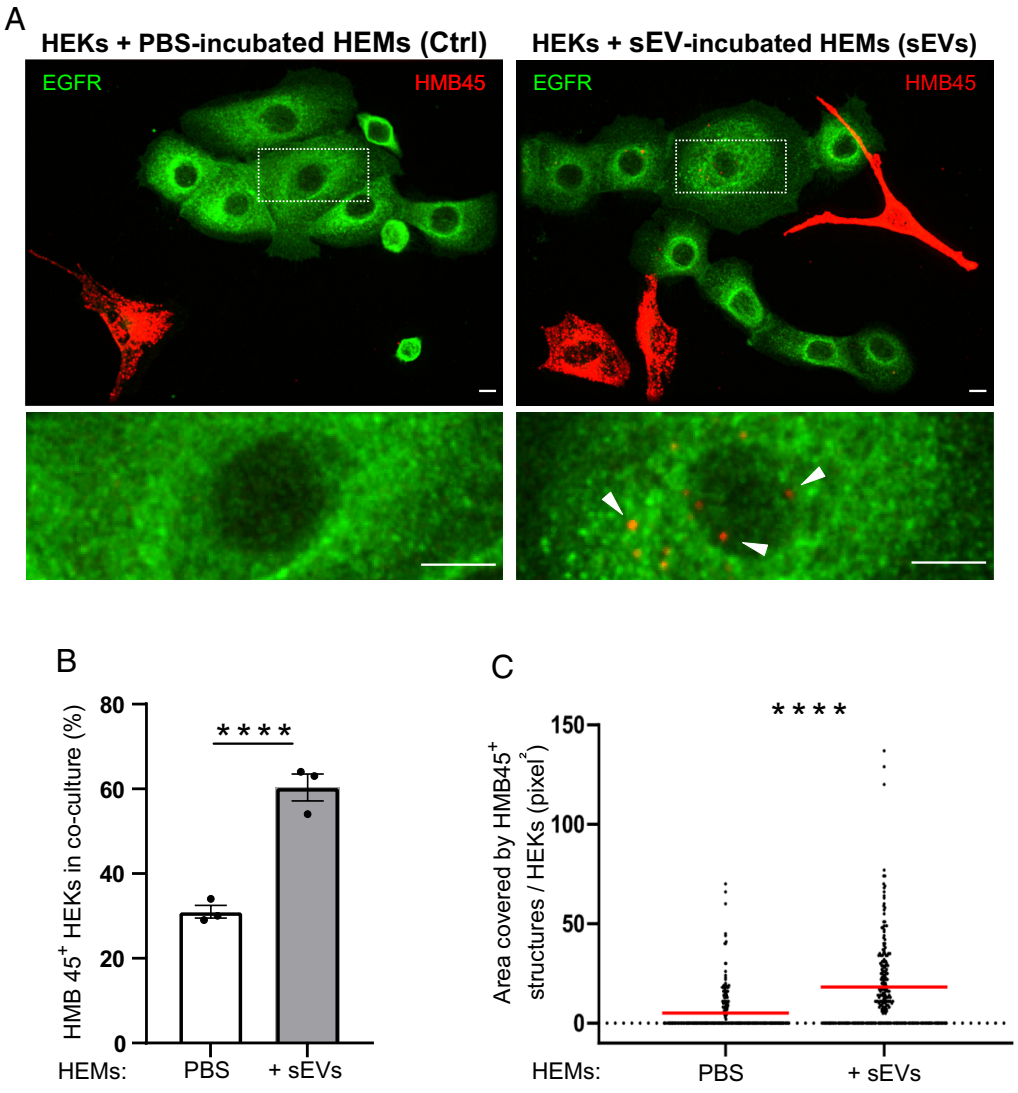

Fig. 1. Keratinocyte-derived sEVs contribute to the transfer of melanin pigment from melanocytes to keratinocytes. (*A*–*C*) HEM-D treated with HEK sEVs (sEVs) or PBS for 48 h were cocultured with HEK-D for 48 h. (*A*) IFM images of cocultures immunolabeled for HMB45 (premelanosome protein, PMEL, red) to label melanin pigment and EGFR (green) to label HEKs. HMB45 staining in HEKs corresponds to transferred melanin pigment. Boxed regions at higher magnification depict the transferred pigment (arrowheads). Bars: 10 μm. (*B*) Quantification of the percentage of HEKs with HMB45-positive structures in each condition. Values are the mean ± SEM of three independent experiments. ****$P < 0.00001$. (PBS, n = 238; sEVs, n = 252). (*C*) Quantification of the area covered by HMB45-positive structures per HEK normalized to the total HEK surface area in each condition. Data shown are the results of three independent experiments with the median indicated in red ****$P < 0.0001$. (PBS, n = 238; sEVs, n = 252).

linked to an increase of Myo Va/F actin colocalization. To test this, HEMs were first immunolabeled with Myo Va and then analyzed by IFM. We found that in both conditions, Myo Va staining was punctate throughout the cytoplasm (Fig. 2*D*, red asterisk). Interestingly, treatment with HEK sEVs enhanced the presence of Myo Va at the dendritic tips (Fig. 2*D*, white arrow). However, when HEMs were incubated with HEK sEVs, quantitative analysis of the signal distribution revealed that sEV exposure specifically promoted a substantial increase in Myo Va intensity at the dendritic tip but did not alter the overall Myo Va intensity in sEV-treated HEMs compared to control (Fig. 2*D* white arrow, Fig. 2 *F* and *G*). This shows that sEVs support the distribution of Myo Va at the tip of HEM dendrites.

Next, the double staining for Myo Va and F-actin showed that at the uppermost tip of sEV-treated HEM dendrites, MyoVa colocalizes with subcortical actin (Fig. 2*E*, white arrow). This was further confirmed by the comparison of normalized Mean Deviation Product (nMDP) values at the tip of dendrites, with the mean nMDP values at the middle and the base of the same dendrite (Fig. 2*H* and *SI Appendix*, Fig. S2*E*). All together, these findings show that HEK sEVs drastically increase melanosome maturation, their accumulation, the buildup of Myo Va at the distal end of the dendrites, and Myo Va/subcortical actin colocalization. Thus, it strongly suggests that HEK sEVs facilitate the peripheral positioning of pigmented melanosomes likely through specific tethering at the dendritic tips.

HEK sEVs Promote Dendrite Outgrowth in Melanocytes. Given that HEK sEVs promote melanosome maturation, accumulation, and positioning of melanosomes as well as their transfer to keratinocytes, we next investigated whether sEVs could also promote per se dendrite formation. In HEMs, the increase of cAMP levels, by promoting cell shape alterations, supports dendrite outgrowth (13, 14, 26). To functionally test the effect of sEVs on the generation of dendrites, we first performed a set of experiments in which we stimulated HEMs with forskolin (FSK), a pharmacological factor that up-regulates the cAMP pathway and known to change HEM morphology (13, 14, 26), followed by IFM analysis using α-tubulin

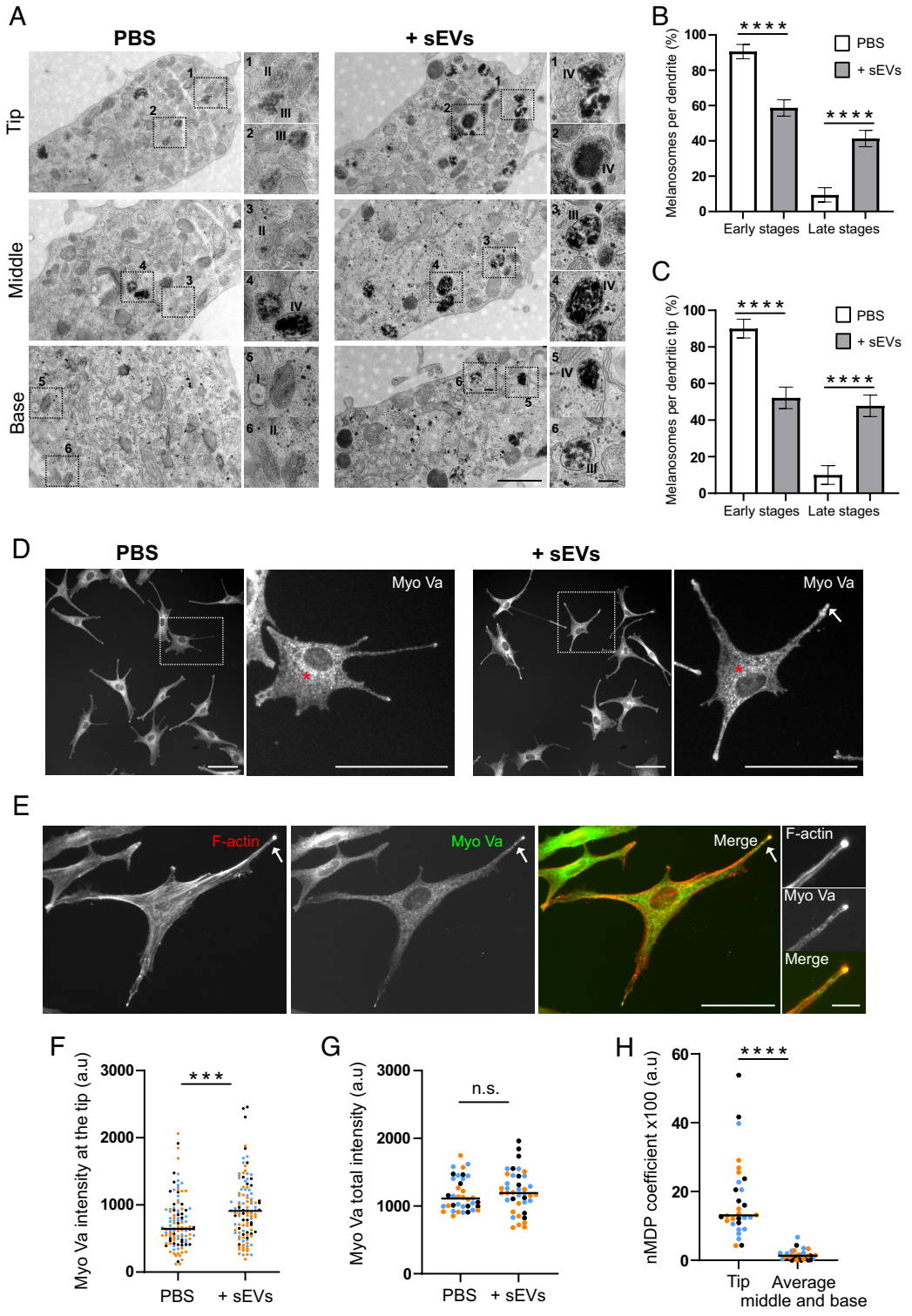

Fig. 2. Keratinocyte sEVs induce melanosome maturation, peripheral accumulation, and increased Myo Va at the tip of melanocyte dendrites. (*A*) Representative conventional TEM micrographs of the tip, middle, and base of HEM-D dendrites incubated for 48 h with PBS or HEK sEVs (sEVs). Insets show magnification of the boxed areas. I to IV depict different stages of maturation of melanosomes. Bars: 1 μm; *Insets*: 200 nm. (*SI Appendix*, Fig. S2 *A* and *B*). (*B* and *C*) Percentage of melanosomes at early and late stages of maturation (*B*) within the dendrites and (*C*) at the dendritic tip of HEM treated as in (*A*).(*B*) PBS: n = 291 melanosomes, 5 dendrites; sEVs: n = 262 melanosomes, 6 dendrites. (*C*) PBS*:* n = 117 melanosomes, 5 dendrites; sEVs: n = 113 melanosomes, 6 dendrites. Values are the mean ± SEM (*****P* < 0.00001). (*D*) IFM images of HEM-D treated as in *A*, immunolabeled for Myo Va (white). Red asterisks point to the punctate Myo Va staining throughout the cytoplasm. Bars: 50 μm; *Insets*: 10 μm. (*E*) IFM image of HEM-D treated with sEVs for 48 h, stained for F-actin (phalloidin, red), and immunolabeled for Myo Va (green). Note the colocalization of Myo Va and F-actin at the dendritic tips (white arrows; *Inset*). Bar: 50 μm; *Inset*: 10 μm. (*F*) Scatter dot plot of Myo Va intensity at the dendritic tip of HEMs incubated as in *A*. Only HEMs with three dendrites were considered. Data shown are the results of three independent experiments (a color per experiment), with the median indicated (n = 112 dendrites). ****P* = 0.0002. (*G*) Scatter dot plot of Myo Va intensity in the whole HEMs (Myo Va total intensity) incubated as in *A*. The same HEMs as in *F* were considered. Data shown are the results of three independent experiments (a color per experiment), with the median indicated (PBS, n = 36 cells; sEVs, n=40 cells). n.s. *P* = 0.4735. (*H*) Scatter dot plot of the normalized Mean Deviation Product coefficient (nMDP) for colocalization of Myo Va with F-actin in HEMs incubated for 48 h with HEK sEVs which exhibited significant accumulation of MyoVa at dendritic tips compared to control (*D*). Comparison of nMDP values at the tip and average nMDP values at the middle and base of the dendrites. Data shown are the results of three independent experiments (a color per experiment), with the median indicated (n = 30 dendrites). *****P* < 0.0001.

and F-actin immunostaining. To evaluate HEM dendricity, we focused exclusively on HEMs with defined extensions emanating from the cell soma (Fig. 3*A*, white arrows), measured their diameter, and considered the diameter of dendrites to be less than or equal to 2 µm, while that of protrusions was larger. We observed that the majority of nonstimulated HEMs (DMSO treated) display the characteristic bipolar morphology with thick protrusions (Fig. 3 *A*, *Left*, red arrows). In contrast, FSK stimulation triggered morphological changes (Fig. 3 *A*, *Right*, blue arrow), resulting in a decrease in the number of HEMs showing protrusions (61% ± 6% vs. 78% ± 8% for DMSO-treated cells) and an increase in the number of dendritic HEMs (88% ± 4% vs. 63% ± 9% for DMSO-treated cells) (Fig. 3 *B* and *C*, two first bars). Moreover, the percentage of FSK-treated HEMs with 2 dendrites was 2.5-fold the percentage for DMSO-treated cells (Fig. 1*D* tenth and ninth bar). When HEMs were incubated with HEK sEVs, HEMs displayed a stellate morphology with dendrites (Fig. 3 *A*, *Bottom*, *Right*, blue arrow), whereas most of the control HEMs (PBS treated) (75% ± 4%) exhibited a spindle shape with protrusions (Fig. 3 *A*, *Bottom*, *Left*, red arrow; B third bar), and 63% ± 7% (Fig. 3*C* third bar), had one or two dendrites (42% ± 3% and 21% ± 4%, respectively) (Fig. 1*D*, seventh and eleventh bar). Importantly, incubation with sEVs promoted a marked increase in the number of dendritic HEMs (about 91% ± 5%) (Fig. 3*C*, last bar) while simultaneously reducing the number of cells with protrusions (about 57% ± 2%) (Fig. 3*B*, last bar). sEV incubation also stimulated de novo dendrite formation, with a higher percentage of cells having 2 dendrites (1.7-fold higher) and 3 to 4 dendrites (6-fold higher) compared to control cells (Fig. 3*D*, twelfth and last bar). To further quantify the observed morphological changes, we used a second approach to measure the Aspect Ratio (AR) (*Materials and Methods*). Reinforcing our findings, the effect of sEVs on HEM dendricity was similar to the effect of FSK and correlated with a significant reduction of the AR ratio, and thereby a higher cell spreading (Fig. 3*E*). Altogether, these data show that the sole incubation with sEVs is sufficient to alter HEM morphology and support dendrite outgrowth to a comparable level to that of FSK. We also noted that the ability of HEK sEVs to promote such dendricity was an intrinsic feature of HEKs and unrelated to their phototypes. Accordingly, a comparable percentage of dendritic HEMs was also observed in HEMs of dark phototype incubated with sEVs from HEK-D (*SI Appendix*, Fig. S2 *C* and *D*). Taken together, these findings underscore the correlation between dendrite formation and morphological changes and indicate that HEK sEVs, independently of HEK skin phototype, bear components that regulate melanocyte function. These results reveal the potency of HEK sEVs as stimulators of HEM dendricity and strongly indicate a potential impact of HEK-sEVs on HEM cytoskeletal organization.

Melanocyte Dendricity Is Mediated by Rac1-Containing Exosomes. The initial process of dendrite formation in human melanocytes requires cytoskeleton reorganization (15) mediated by the cAMP-dependent activation of the small GTP binding protein Rac1 (11, 13, 14). As Rac1-protein is expressed (17) and sequestered in HEKs sEVs (Fig. 4*A*), we wondered whether the Rac1 expression level in HEK sEVs contributes to promote HEM dendricity. First, we evaluated the consequences of Rac1 depletion on HEK morphology and on the quality and quantity of sEVs they secreted using the same experimental approaches as described above (*SI Appendix*, Fig. S1). HEKs were transfected with siRNAs targeting Rac1 (siRac1) or control siRNA (siCtrl). We found that Rac1 silencing significantly reduced both Rac1-protein and Rac1 mRNA levels in cell lysates and sEVs as compared with control (Fig. 4 *A* and *B*). Rac1-depleted HEKs harbored a similar morphology as siCtrl-treated HEKs (*SI Appendix*, Fig. S3*A*), suggesting that depletion of Rac1 did not significantly affect the cytoskeleton and membrane dynamics capacity of HEKs [as shown by IFM (F-actin) and EM; *SI Appendix*, Fig. S3 *A* and *B*]. Moreover, the number and diameter of MVBs (multivesicular bodies) in Rac1-depleted HEKs were similar to control (*SI Appendix*, Fig. S3 *C* and *D*). In addition, sEVs released by Rac1-depleted HEKs were equivalent in number and diameter compared to control (*SI Appendix*, Fig. S3 *E* and *F*). Reinforcing these findings, qualitative, quantitative, and IEM analysis revealed the presence of CD9, CD63, and CD81 in siRac1-sEVS to a comparable extent to siCtrl-sEVs (*SI Appendix*, Fig. S3*G*). We conclude that depletion of Rac1 in HEKs did not impact the general features of sEV such as biogenesis, morphology, quantity, and secretion.

Next, we investigated whether the capacity of HEK sEVs to facilitate HEM dendricity could rely on their Rac1 content. HEMs were incubated with PBS, sEVs released by siCtrl- or siRac1-transfected HEKs. We first checked whether a small amount of siRNA was transferred to HEMs via HEK sEVs, by examining Rac1-protein levels in HEMs incubated with siRac1-sEVs. We found that Rac1 levels were not significantly different compared to HEMs incubated with PBS or siCtrl-sEVs (*SI Appendix*, Fig. S3*H*) ruling out an effect of Rac1 siRNA on Rac1-protein level in HEMs. As expected from data presented in Fig. 3 and *SI Appendix*, Fig. S2 *C* and *D*, HEMs incubated for 48 h with siCtrl-sEVs caused an increase in the average percentage of HEMs harboring dendrites compared to PBS-treated HEMs (71% ± 4% vs. 50% ± 3%, respectively) (Fig. 4 *C* and *D*). Especially, the percentage of HEMs with no dendrites decreased while those with 2 or 3 dendrites increased (Fig. 4*E*), as also reflected by the marked reduction of the AR of HEMs in siCtrl-sEV relative to PBS-treated cells (Fig. 4*F*). In contrast, HEMs treated with siRac1-sEVs lost their ability to promote HEM dendricity. Remarkably, all the analyzed parameters returned to control levels (Fig. 4 *C*–*F*). The results show that HEK-sEVs with reduced Rac1 content fail to promote HEM plasticity and dendrite formation. Taken together, these data substantiate that the molecular content of HEK sEVs, and in particular Rac1, is integrated by HEMs to control dendrite formation, a hallmark of activated HEMs and critical conduits for pigment transfer to HEKs.

Discussion

Skin pigmentation and consequently photoprotection against harmful UV radiations rely on the production and transfer of melanin from HEMs to HEKs. These processes are tightly regulated by a loop of intercellular communication between both epidermal cells. Several reports showed that soluble factors released by HEKs induce and regulate HEM function, including melanin synthesis and transfer. More recent studies have shown that HEKs release sEVs with features of exosomes carrying selected molecules (e.g., miRNAs), that once internalized by HEMs modulate their pigmentation through an increase in melanin production in a phototype-dependent manner (17). In the present study, we demonstrate unique functions of HEK sEVs in stimulating the formation of HEM dendrites, maturation of melanosomes, and their efficient transfer to HEKs.

We show that HEK sEVs induce changes in HEM morphology leading to dendrite formation where mature melanosomes accumulate at their tips, and importantly sEVs promote the transfer of melanin pigment to HEKs. The dendritic process driven by HEK sEVs relies on Rac1-protein which, by modulating actin dynamics and plasma membrane plasticity, endows HEMs with dendrites, special structures for the transfer of melanin pigment

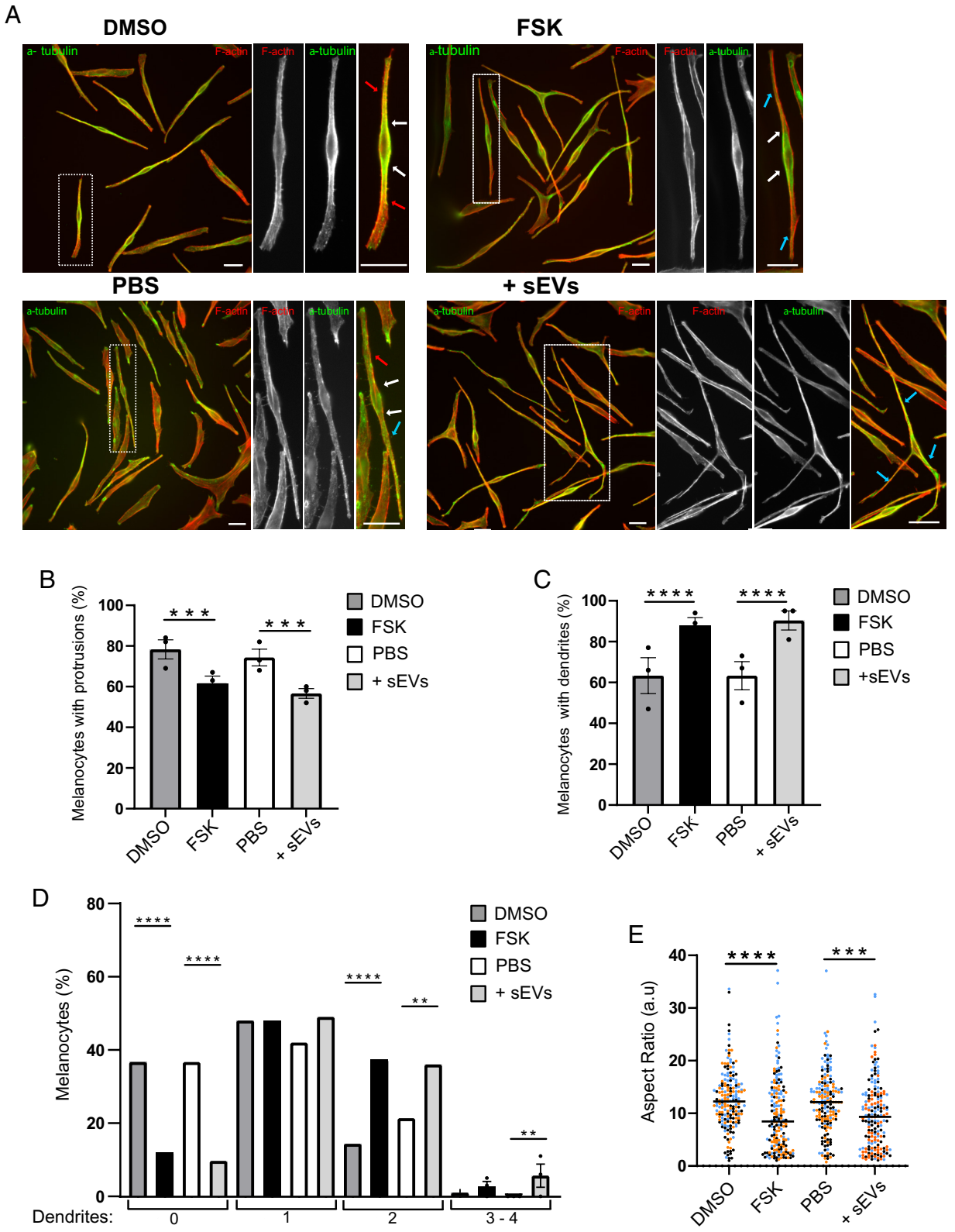

Fig. 3. Keratinocyte sEVs alter melanocyte morphology and promote dendrite outgrowth. (*A*) IFM images of HEM-L treated for 24 h with DMSO or FSK, or for 48 h with PBS or HEK sEVs (sEVs), immunolabeled for α-tubulin (green), and stained for F-actin (phalloidin, red). The boxed regions mark the zoomed area. Bars: 25 μm. Extensions emanating from the cell soma, white arrows; protrusions, red arrows; dendrites, blue arrows. (*B*) Percentage of HEMs [treated as in (*A*)] harboring protrusions (DMSO, n = 186; FSK, n = 187; PBS and sEVs, n = 177). Values are the mean ± SEM of three independent experiments. Only significant *P* values are indicated. ***$P = 5 \times 10^{-4}$. (*C* and *D*) Percentage of HEMs [treated as in (*A*)] showing dendrites (*C*), or 0, 1, 2, or 3 dendrites (*D*) (DMSO, n = 186; FSK, n = 188; PBS, n = 178; sEVs, n = 183). Values are the mean ± SEM of three independent experiments. Only significant *P* values are indicated. (*C*) ****$P = 5.5 \times 10^{-5}$. (*D*) 0 dendrites ****$P = 5.5 \times 10^{-5}$. 2 dendrites, DMSO and FSK, ****$P = 5.3 \times 10^{-5}$; PBS and sEVs, **$P = 0.008$. 3 dendrites, **$P = 0.0032$. *P* values are calculated by comparing the number of dendrites in each category to the sum of the number of dendrites in the other categories. (*E*) Scatter dot plot of the AR of HEMs. Data shown are the result of three independent experiments (a color for each experiment) with the median indicated (DMSO, n = 186; FSK, n = 188; PBS, n = 177; sEVs, n = 183). Only significant *P* values are indicated. DMSO and FSK, ****$P < 0.0001$; PBS and sEVs ***$P = 0.0004$.

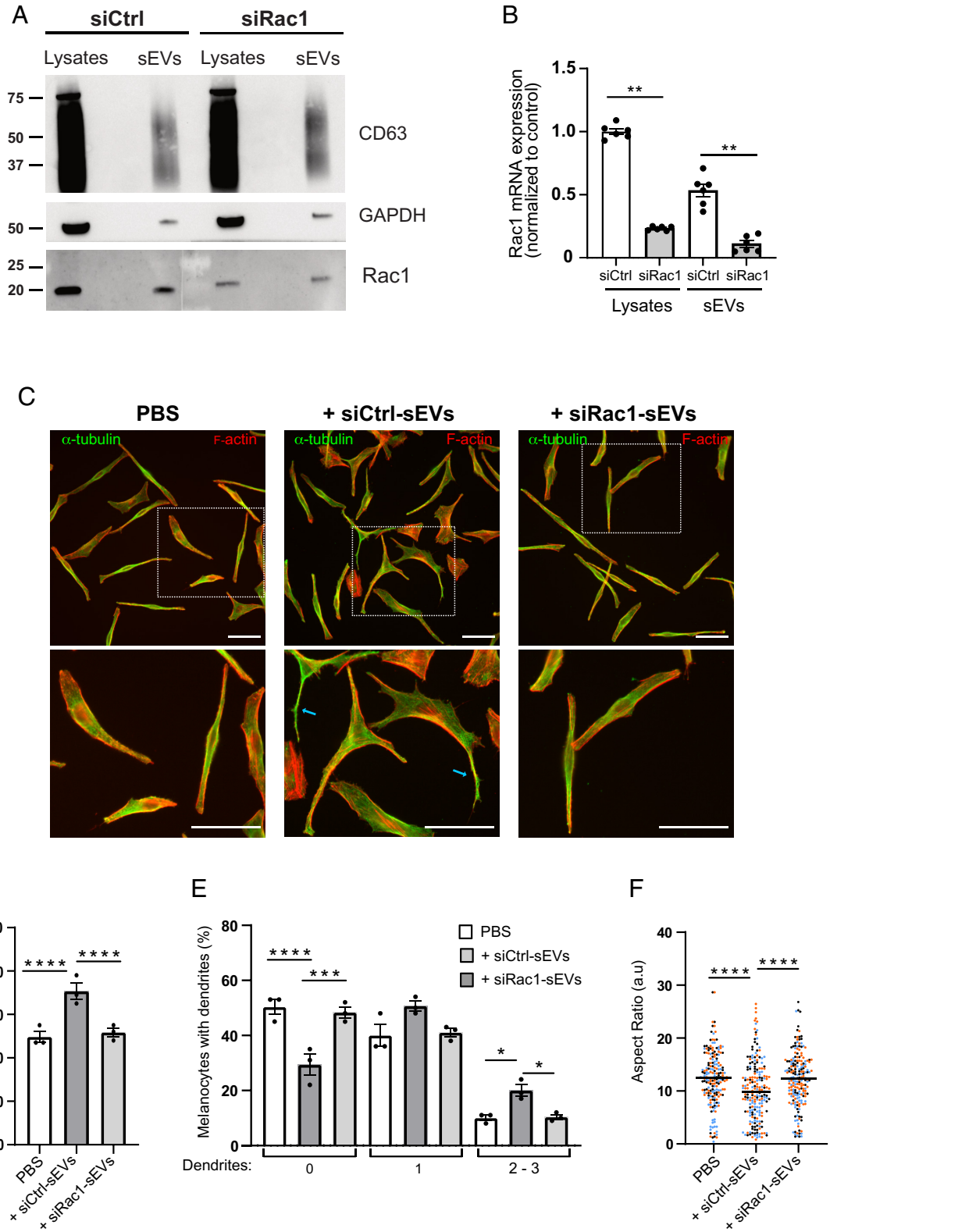

Fig. 4. Melanocyte dendricity is mediated by Rac1-containing sEVs. (*A*) WB analysis of whole-cell lysate (L; 20 μg) and sEVs (sEVs; 10 μg) from siCtrl- and siRac1-transfected HEKs probed with CD63, GAPDH and Rac1 antibodies. Note that since the exposure is the same for the whole WB, the signal for CD63 and GAPDH is slightly saturated for lysates compared with sEVs. (*B*) Quantification of Rac1 mRNA expression normalized to GAPDH in whole-cell lysates and sEVs from siCtrl- or siRac1-transfected HEKs. Values are mean ± SEM of three independent experiments. Only significant *P* values are indicated. ***P* = 0.0022 for whole-cell lysates and sEVs. (*C*) IFM images of HEM-D incubated with PBS, sEVs from HEK transfected with siCtrl (siCtrl-sEVs), or sEVs from HEK transfected with siRac1 (siRac1-sEVs) immunolabeled for α-tubulin (green) and stained for F-actin (red) with fluorescently labeled phalloidin. The boxed regions mark the zoomed area. Blue arrows depict HEM dendrites. Bars, 50 μm. (*D* and *E*) Percentage of HEMs [treated as in (*C*)] with dendrites (*D*) or with 0, 1, or 2 to 3 dendrites (*E*) (PBS, n = 197; + siCtrl-sEVs, n = 206; + siRac1-sEVs, n = 204). Values are the mean ± SEM of three independent experiments. Only significant *P* values are indicated. (*D*) PBS and + siCtrl-sEVs *****P* = 0; + siCtrl-sEVs and + siRac1-sEVs *****P* =0.0001. (*E*) 0 dendrite: PBS and + siCtrl-sEVs *****P* = 0; + siCtrl-sEVs and + siRac1-sEVs ****P* = 0.00045. 2 to 3 dendrites: PBS and + siCtrl-sEVs **P* = 0.0147; + siCtrl-sEVs and + siRac1-sEVs **P* = 0.0191. *P* values are calculated by comparing the number of dendrites in each category to the sum of the number of dendrites in the other categories. (*F*) Scatter dot plot of the AR of HEMs [treated as in (*C*)]. Data shown are the result of three independent experiments (a color for each experiment) with the median indicated. (PBS, n = 197; + siCtrl-sEVs, n = 206; + siRac1-sEVs, n = 204). Only significant *P* values are indicated. *****P* < 0.0001.

to HEKs. These results reinforce and extend previous data showing that HEK sEVs modulate pigmentation via the activation of microphthalmia-associated transcription factor (MITF) (27), by increasing the synthesis and activity of melanosomal enzymes (Tyrp1, Tyr) and pigmentation genes such as Rab27 (17).

In the present study, we show that HEK sEVs induce significant morphological changes in HEMs and dendrite formation, suggesting that sEVs released by HEKs are potent intrinsic activators of dendrite formation. This is first solely due to HEK sEVs, as no soluble factors released by HEKs have been added in these experiments, and second, a specific feature shared by HEKs independently of their skin phototype and without UV irradiation of HEK-L. Presumably, HEK sEVs regulate intracellular trafficking machineries and cytoskeletal organization in HEMs through HEK-specific components enclosed and ferried by sEVs. Importantly, treatment of HEMs with HEK sEVs results in changes in cell shape and in an increase of dendricity in similar proportions to that of FSK treatment of HEMs. Since FSK induces an increase in cAMP production in HEMs that is translated into several processes required for pigmentation, including melanin synthesis and/or melanosome biogenesis and transport (11–13), dendrite formation (this study) and/or melanin transfer, the delivery of HEK sEVs to HEMs could represent a powerful alternative intercellular communication pathway for skin pigmentation and photoprotection. Finally, since high levels of cAMP trigger the upregulation of the active conformation of Rac1 (GTP-bound Rac1) and facilitate its translocation to the plasma membrane where it regulates actin remodeling and membrane plasticity (11–13, 15), it is conceivable that part of HEM activation and responses depends on the levels of Rac1/GTP-Rac1 contained in HEK sEVs and subsequently delivered to HEMs. In line with this, sEVs carrying active Rac-1 protein influence recipient cell behavior (28).

Importantly, we provide evidence that invalidation of Rac1 in HEKs abolishes sEVs-driven morphological changes and dendrite formation in HEMs. The transfer of Rac1 via sEVs may provide a mechanism for delivering Rac1 directly at the sites where dendrites are forming, thereby rapidly orchestrating necessary cytoskeletal rearrangements. Whether Rac1 sequestered in sEVs is under an active or inactive conformation was not investigated due to experimental limitations with primary cells which do not allow preparation of large quantities of sEVs needed to perform such experiments (28). The activation of PKC by ET-1 and phorbol esters has been shown to induce structural changes and dendrite outgrowth in HEMs (10, 13) providing a link between PKC and the modulation of Rac1 activity. PKC might positively regulate Rac1 activation through the recruitment and inhibition of Rac1 GTPase-activating proteins (GAPs) (29). Therefore, different hypotheses could be envisaged. On the one hand, it is possible that Rac1 has been activated in HEK and is present in sEVs under an active conformation to ensure its immediate functionality upon transfer. On the other hand, since our previous proteomic analysis revealed that HEK sEVs also carry PKC (17), it is thus plausible that the spatiotemporal activation of Rac1 takes place in sEVs. Alternatively, activated Rac1 and PKC may be independently delivered by sEVs and activate different signaling pathways that would converge and promote HEM dendricity. Additionally, it is also conceivable that besides Rac1 itself, other Rac1-dependent components or effectors need to be delivered to HEMs for proper functioning. These components could be downstream signaling molecules or regulatory proteins that interact with Rac1 to initiate specific cellular responses. The transfer of Rac1 may be necessary to ensure the availability and proper localization of these components within HEMs. Therefore, the presence of both Rac1 and PKC in sEVs likely provides a more direct avenue to induce dendrite formation, a pivotal mechanism for expanding contacts with HEMs, facilitating pigment transfer.

The effect of HEK sEVs on the remodeling of HEM architecture is certainly a fundamental and basic feature supporting pigmented melanosome transport and transfer to HEKs. In agreement, sEV exposure promotes melanosome maturation and triggers their accumulation and positioning at the tip of HEM dendrites. This is accompanied by the accumulation of Myo Va and its association with subcortical actin at the dendritic tip, suggesting that sEVs contribute to regulating the actin-based melanosome transport and tethering at the dendritic tip before the transfer to neighboring HEKs. Melanocytes exploit Rab27a/melanophilin/Myo Va for the actin-based transport of mature melanosomes to the actin cytoskeleton in dendritic tips. Myo Va colocalizes with melanosomes (6), and pigment cells overexpressing a constitutively active form of Rac1 cause the accumulation MyoVa at dendritic tips (11). The increase of Myo Va distribution at the tip, its association with subcortical actin, and our previous data showing that HEK sEVs increase Rab27a gene expression levels further support the impact of HEK sEVs on HEM pigmentary functions. Together with the presence of Rac1 in sEVs and its role in inducing actin-dependent changes in HEM morphology and melanosome transport along the dendrites, we propose that Rac1 in sEVs is a key component required for the activation of HEM and skin pigmentation.

Melanin transfer to HEKs is a key step in skin pigmentation. The ability of HEK sEVs to promote pigment transfer suggests that sEVs are crucial actors in mediating pigment exchange between these two epidermal cell types. Although the mechanisms of pigment transfer are still debated (30, 31), the generation of dendrites in HEMs is a prerequisite for the establishment of physical contacts with HEKs, while also crucial cellular structures for pigment positioning, enrichment, and transfer, further supporting that sEVs-induced HEM plasticity is pivotal to support these pigmentary functions. In agreement, maintaining the capacity of HEMs to remodel their plasma membrane and to contact HEKs is key for melanin transfer (32). In addition, this process can rely on HEK-secreted factors (soluble factors and EVs) and components, such as miRNAs (32), known to be enclosed in HEK exosomes (17). Therefore, and despite the lack of evidence in three-dimensional (3D) skin tissue system, HEK-derived sEVs may likely cooperate with soluble factors secreted by HEKs to synergize the capacity of HEMs to produce pigment, to provide melanin to HEKs, and to color and photoprotect the skin.

In sum, we propose that sEVs secreted by HEKs and their associated content instruct HEMs so that they integrate and translate these signals into cellular and molecular processes promoting HEM activation. As such, sEVs regulate the expression of melanogenic enzymes and melanosome-associated machineries (17), the remodeling of cell architecture through dendrite formation, the transport and peripheral positioning of pigmented melanosomes to the dendritic tips, and importantly, the transfer of melanin pigment to HEKs (this study). Consequently, HEK-derived sEVs are major regulators of intercellular communication in skin cells and critical actors of the normal skin. Considering that human pigmentation is pivotal to protect the skin against UV solar radiations, and bearing in mind that defects in cutaneous pigmentation lead not only to pigmentary disorders but can also contribute to several skin cancer types, including melanoma, our study opens up broad perspectives for investigating the contribution of the sEVs-mediated HEM functions to such physiological and pathological processes.

Materials and Methods

Antibodies. The following antibodies were used for immunoblotting (WB), IF, or immunoelectron microscopy (IEM): rabbit (rb) anti-β-tubulin (Abcam ab59680; 1:500; WB); rb anti-GAPDH (Sigma G9545, 1:10,000; WB); rb Syntenin (Abcam ab133267;1:1,000; WB); rb Calnexin (Enzo ADI-SPA-860; 1:1,000; WB); rb anti-Alix (Abcam ab186429; 1:1,000; WB); mouse (ms) monoclonal anti-β-actin (Sigma clone AC-74, 1:10,000; WB), ms monoclonal anti-TSG101 (GeneTex, GTX70255; 1:500; WB) or (Santa Cruz, C-2, sc-7964; 1:200 WB); ms anti-Rac1 (Millipore clone 23A8; 1:1,000; WB); ms anti-human CD81 monoclonal antibody (Millipore CLB579; 1:1,000; WB); ms Anti-CD9 (Sigma-Aldrich, clone MM2/57 CLB 162; 1:1,000; WB); ms monoclonal CD63 (Invitrogen, 1:200; WB, IEM); rb anti-MyosinVa (Cell Signaling 3402S; 1:50; IF); sheep anti-EGFR (Fitzgerald 20-ES04, 1:400 IF); ms anti-HMB45 (Abcam ab787; 1:200; IF); ms DM1A α Tubulin (Sigma-Aldrich T6199; 1,200; IF); rb CD9 (Abcam ab236630; 1:80; IEM); rb CD81 (Abcam ab233692; 1:50; IEM); and rb anti-mouse Fc fragment (Dako Agilent Z0412; 1:200; IEM). Secondary antibodies coupled to Horseradish peroxidase (HRP)-conjugated goat polyclonal antibodies to rabbit IgG (Abcam ab6721) or to mouse IgG (Abcam ab6789) were used at 1:5,000. Secondary goat anti-rabbit or anti-mouse antibodies conjugated to Alexa Fluor 488, 555, or 647 were from Invitrogen and used at 1:200. Alexa Fluor™ 647 Phalloidin (Thermo Fisher, A22287).

Cell Culture. Normal from HEM-D or HEM-L phototypes and normal HEKs from HEK-D or HEK-L phototypes used in this study were isolated from the neonatal foreskin. HEMs were purchased from PromoCell or Tebu-Bio, and HEKs were purchased from CellSystems or Sterlab. HEMs and HEKs were used from passages one to four and maintained in culture in DermaLife Basal Medium supplemented with DermaLife M Life factors (melanocytes-supplemented medium) or with DermaLife K Life factors (keratinocytes supplemented medium), respectively.

To assess HEM dendricity, HEMs (10^4 or 1.5×10^4 cells) cultured in 0.5 mL of HEM-supplemented medium (followed 5 h later by a PBS rinse) were incubated for 48 h in 0.5 mL of HEM-supplemented medium with HEK sEVs (2×10^5 particles/cell or 4×10^3 particles/cell from OptiPrep purified sEVs), or with the same volume of PBS as a control, or for the last 24 h of the experiment with 30 μM of FSK (Sigma-Aldrich F6886), dissolved in dimethyl sulfoxide (DMSO, Sigma-Aldrich, CAS 67-68-5), or with 0.6% DMSO as a control vehicle for FSK. The cells were then processed for microscopy analysis.

Of note, to be as close as possible to the ratio of HEMs and HEKs present in the epidermis (ratio 1:36) (1), one HEM was incubated with sEVs recovered from 20 HEKs from donors of the same phototype. A higher concentration was toxic for the HEMs.

To evaluate pigment transfer from HEMs to HEKs, 10^5 HEMs cultured in HEM-supplemented medium (followed 5 h later by a PBS rinse) were incubated with HEK sEVs (3×10^9 particles) or PBS for 48 h in 1 mL HEM-supplemented medium, trypsinized, and cocultured with HEKs at ratio 1:1 in HEM-supplemented medium for 2 d before fixation.

Conditioned Media (CM). The CM were recovered from cultured HEKs. Before recovering the CM, cells were washed once with PBS and cultured subconfluently in fresh HEK-supplemented medium for 48 h in T150 or T75 cell culture flasks.

siRNA Transfection. HEKs (1.25×10^5 cells) were seeded in 100 mm dish and transfected with 40 nM of siRNA using Oligofectamine (Invitrogen) according to the manufacturer's instructions using nontargeting siRNA (siCtrl: 5′-AATTCTCCGAACGTGTCACGT-3′) or siRNA targeting the Rac1-protein (siRac1: 5′-ATGCATTTCCTGGAGAATATA-3′) from Qiagen. Cells were transfected twice: the first shot of transfection 24 h after seeding, followed by a second shot 48 h after the first shot. Four hours after each transfection, the medium was removed and replaced by fresh HEK-supplemented medium (12 mL/dish). CM from each condition was recovered 48 h after the second transfection to isolate sEVs.

Quantitative Real-Time PCR (qPCR). Total RNA was extracted from transfected HEKs (i.e., siRNA Ctrl or siRNA targeting Rac1) or HEK sEVs from transfected HEKs (siRNA Ctrl or siRNA targeting Rac1 using the RNA extraction kit (MACHEREY-NAGEL) or total exosome RNA kit (4478545, ThermoFisher). The cDNA was generated from 0.3 μg of RNA using the SuperScript First-Strand Synthesis System (11904-018, Invitrogen) following the manufacturer's protocols. qPCR was performed using the LightCycler 480 SYBR Green I Master (Roche) on plate-based qPCR amplification and detection instrument LightCycler 480 (Roche). GAPDH was used as an endogenous normalizer. Primers for Rac1: Fw 5′-ATGTCCGTGCAAAGTGGTATC-3′; Rev 5′-CTCGGATCGCTTCGTCAAACA-3′. GAPDH: Fw: 5′-CTGGGCTACACTGAGCACC- 3′; Rev 5′- AAGTGGTCGTTGAGGGCAATG-3′. Experiments were performed with at least three biological replicates. The method ΔΔCT was used to obtain the relative expression levels, and the ratio between the control and gene of interest was calculated with the formula $2^{-\Delta\Delta CT}$.

sEVs Isolation by Differential Ultracentrifugation. sEVs were prepared from CM for 48 h of 70 to 90% confluent HEKs. Briefly, CM were centrifuged at 300 g for 10 min at 4 °C. Next, the supernatant was centrifuged at 2,000 g for 20 min at 4 °C to remove debris. Then, the supernatant was centrifuged at 10,000 g for 30 min (4 °C), and the sEVs were collected from the supernatant by centrifugation at 100,000 g for 60 min (4 °C) in a Ti45 rotor (Beckman). The pellet was resuspended and washed in PBS, pH 7.5, and recentrifuged at 100,000 g for 60 min (4 °C), in a Ti70 rotor (Beckman). The resulting pellet was resuspended in PBS and stored at −80 °C.

For the OptiPrep density gradient, a discontinuous iodixanol gradient was prepared, 40, 20, and 10% from a stock solution (OptiPrep™ Density Gradient Medium; Sigma-Aldrich; D1556), with 0.25 M sucrose, 10 mM Tris pH 8, and 1 mM EDTA. The 100,000 g pellet was laid at the bottom of the gradient to obtain a 40% fraction and centrifuged at 100,000 g for 18 h at 4 °C in a SW41 Ti rotor (Beckman), stopping without brake. Ten fractions of 490 μL each were collected. The fractions were diluted in PBS, centrifuged at 100,000 g in an SW 32 Ti rotor (Beckman) for 60 min at 4 °C, resuspended in equal volumes of PBS, and stored at −80 °C.

sEV Quantification by NTA. The isolated sEVs were diluted 1:1,000 in filtered PBS and loaded into the sample chamber. NTA was performed using ZetaView PMX-120 (Particle Metrix) with software version 8.04.02. The instrument settings were at 22°C, sensitivity of 75, and shutter of 75. Measurements were done using two different dilutions at 11 different positions (two cycles per position) and a frame rate of 30 frames per second.

Electron Microscopy.

TEM of sEVs. Pellets resuspended in PBS were processed as previously described and according to the MISEV guidelines. Briefly, 5 μL of sEVs was deposited on Formvar-carbon-coated electron microscopy grids incubated for 20 min at room temperature (RT) and fixed in 2% paraformaldehyde (PFA) in phosphate buffer (PB 0.2 M, pH 7.4). After 20 min at RT, samples were washed 6 times with H_2O and postfixed in 1% glutaraldehyde in PBS for 5 min at RT. For negative contrast, the grids were placed on a drop of 4% uranyl acetate (UA) and 2% methylcellulose (MC) at 2% (ratio of 1 UA: 9 MC) for 10 min on ice. The excess was then removed by blotting on Whatman paper and dried for 30 min at RT. All these steps were done in the dark.

Immunolabeling electron microscopy (IEM) of sEVs. Five microliters of sEVs was loaded on grids and fixed with 2% PFA in PB (0.2 M, pH 7.4) for 20 min at RT. Immunodetection was performed with a mouse monoclonal CD63, a rabbit CD9, or a rabbit CD81 diluted in 1% BSA/PBS for 60 min at RT. Secondary incubation was next performed with a rabbit anti-mouse Fc fragment (Dako Agilent Z0412; 1:200) for CD63 for 20 min, at RT. Grids were incubated for 20 min with Protein A-Gold 10 nm diluted in 1% BSA/PBS (1:50) (Cell Microscopy Center, Department of Cell Biology, Utrecht University). A second fixation step with 1% glutaraldehyde in PBS was performed. Grids were contrasted with UA and MC as for TEM. All samples were examined with a Tecnai Spirit electron microscope (FEI, Eindhoven, The Netherlands), and digital acquisitions were made with a numeric 4k CCD camera (Quemesa, Olympus, Münster, Germany).

TEM of cells. HEKs or HEMs were fixed in 2.5% (v/v) glutaraldehyde, 2% PFA in 0.1 M cacodylate buffer for 24 h, postfixed with 1% (w/v) osmium tetroxide supplemented with 1.5% (w/v) potassium ferrocyanide, dehydrated in ethanol, and embedded in Epon as previously described (33). Ultrathin EPON sections (60 nm) of cell monolayers were prepared, contrasted with UA and lead citrate, and observed at an 80 kV transmission electron microscope (Tecnai Spirit G2; Thermo Fisher Scientific) equipped with a 4k CCD camera (Quemesa, Soft Imaging System). Images were analyzed with iTEM software (EMSIS), and statistical analysis was done by GraphPad Prism.

WB Analysis. Cells were lysed on ice in lysis buffer (20 mM Tris pH 7.5, 150 mM NaCl, 1% Triton X-100, and 1 mM ethylenediaminetetraacetic acid (EDTA), pH 8) with a protease inhibitor cocktail (Roche). Whole-cell lysates or sEVs were

incubated in sample buffer with or without DTT (400 mM) (Sigma), boiled for 5 min and fractionated with sodium dodecyl sulfate–polyacrylamide gel electrophoresis (SDS-PAGE) using NuPAGE (4 to 12%) Bis-Tris gels (Invitrogen), and transferred to nitrocellulose membranes (Millipore). The membranes were blocked in PBS/Tween 0.1% (PBS/T) with 5% nonfat dried milk, incubated with the indicated primary antibody diluted in the same solution, washed three times in PBS/T, and incubated with HRP-conjugated secondary antibody followed by washing in PBS/T. To reveal the membranes, SuperSignal™ West Pico PLUS Chemiluminescent (ThermoFisher) was used.

Images of immunoblots were captured with ChemiDoc Touch Bio-Rad 2 or with CL-XPosure Film (ThermoFisher scientific) within the linear range and quantified by densitometry using the "analyze gels" function in ImageJ (https://imagej.net/ij/).

IFM. Cell seeded on glass coverslips were fixed with 2% (v/v) PFA in PBS at room temperature for 15 min and then washed three times in PBS and once in PBS with 50 mM glycine. Dilutions of primary and secondary antibodies were prepared in buffer A: PBS with 0.2% (w/v) Bovine Serum Albumin (BSA) and 0.1% (w/v) saponin. The coverslips were incubated with the primary antibodies for 1 h at room temperature after being washed once in buffer A. Coverslips were washed three times in buffer A, followed by incubation with secondary antibodies and phalloidin for 45 min if necessary. The final washing steps were performed three times in buffer A, once in PBS, and once in water. The coverslips were mounted on glass slides using ProLong™ Gold Antifade Mount with DAPI (Thermo Fisher Scientific).

Image Acquisition. Epifluorescence microscopy was carried out with a Histo-Epifluo Nikon Microscope (Nikon NIe with camera CCD CoolSnap HQ2 and color CMOS sensor DS-Ri2 from Nikon) (Figs. 3*A* and 4*A*) and a Leica DM6B microscope equipped with a 40× NA 1.3 oil immersion objective and a sCMOS camera (Fig. 2 *D* and *E* and *SI Appendix*, Figs. S2*D* and S4*A*). Spinning-disc confocal microscopy was carried out with a Yokogawa CSU-X1 on a Nikon Inverted Eclipse TI-E microscope equipped with a 40× NA 1.3 oil immersion objective and a sCMOS Prime 95B (Photometrics) (Fig. 1*A*). 3D reconstructions were generated by using the software Fiji (https://fiji.sc/).

Image Analysis and Quantification.

Dendrite/protrusion size measurement. The diameter of dendrites or protrusions was measured using the Fiji software's (34) "straight" tool. The AR was measured using Fiji software's "fit ellipse" function which displays the major and minor axis for each cell.

Myo Va and F-actin colocalization. Regions of interest (ROI) were manually drawn at the tip of each dendrite, and the same ROI was used to quantify the colocalization values at the tip, middle, and base of the same dendrite. Colocalization values were measured using the Colocalization Colormap plugin developed for Fiji (35). This plugin calculates the nMDP for each pixel in the image, reflecting the correlation between intensities in the Myo Va (Cy3) and F-actin (Cy5) channels. The nMDP values were normalized by the maximum values.

Measurement of Myo Va intensity. A manually drawn ROI with a diameter of 11.3 μm was used to measure in Cy3 images the mean intensity of Myo Va at the tip of each dendrite, as well as the mean background intensity near the same dendrite for all dendrites analyzed. The plotted values correspond to the mean Myo Va intensity at the tip after background subtraction. A manually drawn ROI of the area of each cell was used to measure in Cy3 images the mean intensity of MyoVa in the whole cell, as well as the mean background intensity near the same cell for all the cells analyzed. The plotted values correspond to the mean total Myo Va intensity in the cell after background subtraction.

Quantification of pigment transfer. A Fiji macro was written to perform the analysis on maximum intensity Z projections. The HMB45-positive structures were counted in manually drawn ROI delineating cell contours using ImageJ's Find Maxima function to identify local maxima. The surface area of these structures was extracted using the Li global threshold method, which minimizes the cross-entropy between the background and the foreground averages, to calculate the proportion of the cell surface area covered by the transferred pigment. HMB45-positive structures at the top of the cells were excluded from quantification.

Measurement of MVB. Quantification of MVB size and number was determined using the iTEM (Soft Imaging System) software.

Statistical Analysis. We used GraphPad Prism version 9.0.0 for Windows, GraphPad Software, San Diego, California USA, (www.graphpad.com) for statistical analysis. To compare two conditions, we performed a nonparametric Mann–Whitney test (Figs. 1*C*, 2 *F*, *G*, and *H*, and 4*B*) or an unpaired *t* test (*SI Appendix*, Figs. S1*D* and S3 *C*, *D*, *F*, and *H*). To compare three or more conditions (Figs. 3*E* and 4*F*), we used a nonparametric Kruskal–Wallis test, followed by Dunn's multiple comparison test. For percentage comparisons (Figs. 1*B*, 2 *B* and *C*, 3 *B–D*, 4 *D* and *E* and *SI Appendix*, Fig. S2 *C* and *D*), we applied Fisher's exact test (https://www.socscistatistics.com/tests/chisquare2/default2.aspx), with application of the Benjamini–Hochberg multiple comparison correction (https://www.sdmproject.com/utilities/?show=FDR) when necessary.

Data, Materials, and Software Availability. All study data are included in the article and/or *SI Appendix*.

ACKNOWLEDGMENTS. We thank Dr. C. Delevoye, Dr. P. Stahl, and Dr. Ph. Vernier for insightful discussions and critical reading of the manuscript. This work was supported by the CNRS, the Foundation for Medical Research (FRM EQU201903007827), the European Union, EVCA Twining project (Horizon GA no. 101079264), the European Union's Horizon 2020 research and innovation programme under the Marie Skłodowska-Curie (Grant agreement no. 847718)", and the Cell and Tissue Imaging core facility (PICT IBiSA, Institut Curie), member of the French National Research Infrastructure France-BioImaging (ANR10-INBS-04). C.G. was a recipient of a postdoctoral fellowship from the Foundation for Medical Research (FRM SPF201809006932). M.G.-D. was supported by PhD fellowship from Institut Curie EuReCa PhD Programme (Grant agreement no. 847718).

1. T. B. Fitzpatrick, A. S. Breathnach, The epidermal melanin unit system. *Dermatol. Wochenschr.* **147**, 481–489 (1963).
2. Y. Yamaguchi, M. Brenner, V. J. Hearing, The regulation of skin pigmentation. *J. Biol. Chem.* **282**, 27557–27561 (2007).
3. G. Raposo, D. Tenza, D. M. Murphy, J. F. Berson, M. S. Marks, Distinct protein sorting and localization to premelanosomes, melanosomes, and lysosomes in pigmented melanocytic cell. *J. Cell Biol.* **152**, 809–824 (2001).
4. C. Delevoye, M. S. Marks, G. Raposo, Lysosome-related organelles as functional adaptations of the endolysosomal system. *Curr. Opin. Cell Biol.* **59**, 147–158 (2019).
5. V. Tsakraklides *et al.*, Subcellular localization of GFP-myosin-V in live mouse melanocytes. *J. Cell Sci.* **112**, 2853–2865 (1999).
6. X. S. Wu *et al.*, Identification of an organelle receptor for myosin-Va. *Nat. Cell Biol.* **4**, 271–278 (2002).
7. A. N. Hume *et al.*, Rab27a regulates the peripheral distribution of melanosomes in melanocytes. *J. Cell Biol.* **152**, 795–808 (2001).
8. T. Hirobe, Stimulation of dendritogenesis in the epidermal melanocytes of newborn mice by melanocyte-stimulating hormone. *J. Cell Sci.* **33**, 371–383 (1978).
9. P. R. Gordon, C. P. Mansur, B. A. Gilchrest, Regulation of human melanocyte growth, dendricity, and melanization by keratinocyte derived factors. *J. Invest. Dermatol.* **92**, 565–572 (1989).
10. M. Hara, M. Yaar, B. A. Gilchrest, Endothelin-1 of keratinocyte origin is a mediator of melanocyte dendricity. *J. Invest. Dermatol.* **105**, 744–748 (1995).
11. G. A. Scott, L. Cassidy, Rac1 mediates dendrite formation in response to melanocyte stimulating hormone and ultraviolet light in a murine melanoma model. *J. Invest. Dermatol.* **111**, 243–250 (1998).
12. M. Yaar, B. A. Gilchrest, Ageing and photoageing of keratinocytes and melanocytes. *Clin. Exp. Dermatol.* **26**, 583–591 (2001).
13. G. Scott, Rac and rho: The story behind melanocyte dendrite formation. *Pigment Cell Res.* **15**, 322–330 (2002).
14. G. Scott, S. Leopardi, The cAMP signaling pathway has opposing effects on Rac and Rho in B16F10 cells: Implications for dendrite formation in melanocytic cells. *Pigment Cell Res.* **16**, 139–148 (2003).
15. R. D. Evans *et al.*, Myosin-Va and dynamic actin oppose microtubules to drive long-range organelle transport. *Curr. Biol.* **24**, 1743–1750 (2014).
16. C. Chavez-Muñoz, J. Morse, R. Kilani, A. Ghahary, Primary human keratinocytes externalize stratifin protein via exosomes. *J. Cell Biochem.* **104**, 2165–2173 (2008).
17. A. Lo Cicero *et al.*, Exosomes released by keratinocytes modulate melanocyte pigmentation. *Nat. Commun.* **6**, 7506 (2015).
18. M. Jiang *et al.*, Keratinocyte exosomes activate neutrophils and enhance skin inflammation in psoriasis. *FASEB J.* **33**, 13241–13253 (2019).
19. G. van Niel, G. D'Angelo, G. Raposo, Shedding light on the cell biology of extracellular vesicles. *Nat. Rev. Mol. Cell Biol.* **19**, 213–228 (2018).
20. G. van Niel *et al.*, Challenges and directions in studying cell–cell communication by extracellular vesicles. *Nat. Rev. Mol. Cell Biol.* **23**, 369–382 (2022).
21. Y. Liu *et al.*, Exosomal miRNA derived from keratinocytes regulates pigmentation in melanocytes. *J. Dermatol. Sci.* **93**, 159–167 (2019).
22. K. Takano *et al.*, Quantitative changes in the secretion of exosomes from keratinocytes homeostatically regulate skin pigmentation in a paracrine manner. *J. Dermatol.* **47**, 265–276 (2020).
23. C. Théry *et al.*, Minimal information for studies of extracellular vesicles 2018 (MISEV2018): A position statement of the International Society for Extracellular Vesicles and update of the MISEV2014 guidelines. *J. Extracell Vesicles* **7**, 1535750 (2018).

24. X. Wu, J. A. Hammer, Melanosome transfer: It is best to give and receive. *Curr. Opin. Cell Biol.* **29**, 1–7 (2014).
25. L. Ripoll *et al.*, Myosin VI and branched actin filaments mediate membrane constriction and fission of melanosomal tubule carriers. *J. Cell Biol.* **217**, 2709–2726 (2018).
26. R. Buscà, R. Ballotti, Cyclic AMP a key messenger in the regulation of skin pigmentation. *Pigment Cell Res.* **13**, 60–69 (2000).
27. S. Shibahara *et al.*, Regulation of pigment cell-specific gene expression by MITF. *Pigment Cell Res.* **13**, 98–102 (2000).
28. S. K. Gopal *et al.*, Oncogenic epithelial cell-derived exosomes containing Rac1 and PAK2 induce angiogenesis in recipient endothelial cells. *Oncotarget* **7**, 19709–19722 (2016).
29. X. Tu, R. Yasuda, L. A. Colgan, Rac1 is a downstream effector of PKCα in structural synaptic plasticity. *Sci. Rep.* **10**, 1777 (2020).
30. L. Bento-Lopes *et al.*, Melanin's journey from melanocytes to keratinocytes: Uncovering the molecular mechanisms of melanin transfer and processing. *Int. J. Mol. Sci.* **24**, 11289 (2023).
31. S. Benito-Martínez, L. Salavessa, G. Raposo, M. S. Marks, C. Delevoye, Melanin transfer and fate within keratinocytes in human skin pigmentation. *Integr. Comp. Biol.* **61**, 1546–1555 (2021).
32. L. Domingues *et al.*, Coupling of melanocyte signaling and mechanics by caveolae is required for human skin pigmentation. *Nat. Commun.* **11**, 2988 (2020).
33. I. Hurbain *et al.*, Electron tomography of early melanosomes: Implications for melanogenesis and the generation of fibrillar amyloid sheets. *Proc. Natl. Acad. Sci. U.S.A.* **105**, 19726–19731 (2008).
34. J. Schindelin *et al.*, Fiji: An open-source platform for biological-image analysis. *Nat. Methods* **9**, 676–682 (2012).
35. A. Gorlewicz *et al.*, Colocalization colormap–An imagej plugin for the quantification and visualization of colocalized signals. *Neuroinformatics* **18**, 661–664 (2020).